ARCHIVES OF ACOUSTICS
34, 4, 697–714 (2009)

Experimental Study of Simultanoeus Transmission of a Light Wave and an Ultrasonic Wave in an Optical Fiber with the use of a Mach–Zehnder Interferometer

Sylwia MUC, Tadeusz GUDRA, Elżbieta BEREŚ–PAWLIK

Wrocław University of Technology
Institute of Telecomunications, Teleinformatics and Acoustics
Wybrzeże Wyspiańskiego 27, 50-370 Wrocław, Poland
e-mail: sylwia.muc@pwr.wroc.pl

(*received April 8, 2009; accepted November 13, 2009*)

The possibility of acoustic wave propagation in optical waveguides creates new prospects for the simultaneous use of a light wave and an ultrasonic wave in, for instance, medicine for cutting biological tissues with a surgical ultrasonic laser knife. A Mach–Zehnder optical waveguide interferometer was used in the experimental studies of simultaneous transmission of those two wave types. If ultrasonic vibrations are delivered to one of the interferometer arms, a light modulation effect is produced. This paper presents measurement results for different methods of delivering ultrasonic waves to the optical fiber, i.e. using radial vibrations of a piezoelectric disk or longitudinal vibrations generated by a sandwich ultrasonic transducer with a velocity transformer.

Keywords: laser-ultrasound transmission in optical fiber, Mach–Zehnder interferometer.

1. Introduction

The possibility of acoustic wave propagation in optical waveguides creates new prospects for the simultaneous use of a light wave and an ultrasonic wave in, for instance, medicine for cutting biological tissues. Laser and ultrasonic technologies complement each other and during a medical procedure those two methods are very often applied simultaneously using separate standard devices. The benefits of combining the two technologies were described in [1]. The mathematical model of a monomode Mach–Zehnder interferometer and the principle of operation it is known and was described in literature [2, 3, 5, 6]. For monomode techniques a general formalism describing their optical characteristics was presented in the same literature too.

2. Mathematical model of a monomode Mach–Zehnder interferometer

Figure 1 shows a model of the monomode Mach–Zehnder interferometer [2].

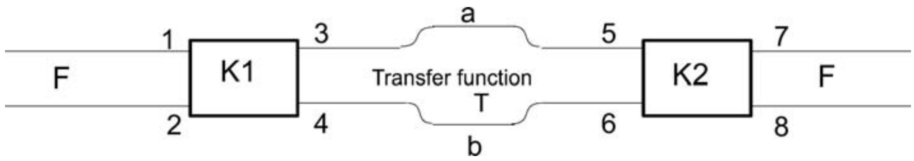

Fig. 1. Model of the Mach–Zehnder interferometer.

The transfer function of the couplers ($K1$ and $K2$) are described by the matrices K_1 and K_2, respectively. Matrix T is a propagation matrix (a transfer function) describing the sensitivity of the interferometer. T describes waveguides a and b. In the general case, all the waveguides and components are considered to be birefringent. The output field is given by [2]:

$$\mathbf{F}_{\text{out}} = K_2 T K_1 \mathbf{F}_{\text{in}}, \tag{1}$$

where $\mathbf{F}_{\text{out}}$ – the output field, $\mathbf{F}_{\text{in}}$ – the input field.

The matrix T is expressed by the formula:

$$T = a \exp(i\phi_1) B, \tag{2}$$

where a – scalar transmittance, ϕ_1 – phase delay, B – a Jones matrix describing the birefringence of the system.

The sensing mechanisms of the monomode interferometer are based on the modulation of one of the parameters: a, ϕ_1, B or on a combination of these parameters. In practice, monomode interferometers are based on phase or polarization modulations. For a fiber with perfect cylindrical symmetry, B becomes identical with matrix 1. Since birefringence effects within the fiber must be taken into account, The B matrix, for example for a linearly birefringent fiber, is expressed by the formula [2, 7]:

$$B = \begin{bmatrix} \exp\left(\dfrac{i\phi_2}{2}\right) & 0 \\ 0 & \exp\left(\dfrac{-i\phi_2}{2}\right) \end{bmatrix} \tag{3}$$

$\mathbf{F}_{\text{out}}$ and $\mathbf{F}_{\text{in}}$ are four-element vectors. $\mathbf{F}_{\text{in}}^{\text{T}} = (E_{1X}, E_{1Y}, E_{2X}, E_{2Y})$, where the indexes 1 and 2 represent the electric fields at ports 1 and 2, respectively, while x and y represent the orthogonal transverse field components. The matrices K can be expressed by [2]:

$$K_1 = \begin{bmatrix} K_{13} & K_{14} \\ K_{23} & K_{24} \end{bmatrix}, \tag{4}$$

$$K_2 = \begin{bmatrix} K_{57} & K_{58} \\ K_{67} & K_{68} \end{bmatrix}. \tag{5}$$

For matrix T we can write similarly:

$$T = \begin{bmatrix} T_{aa} & T_{ab} \\ T_{ba} & T_{bb} \end{bmatrix}, \tag{6}$$

where

$$T_{ij} = \widehat{T}_{ij} \exp(it_{ij}) T_{ij}, \tag{7}$$

$$t_{ij} = \phi_{ij} + i\varphi_{ij}, \tag{8}$$

T_{aa} T_{bb} – transfer functions for the spatially distinct waveguides a and b, T_{ab} – represents the coupling between the waveguides, $\widehat{T}_{ij}$ – a Jones matrix, t_{ij} – complex transmittance in which there is a phase delay and a φ_{ij} – attenuation.

It is most often assumed that $T_{ab} = T_{ba} = 0$.

Assuming that the fiber is ideal (its components are not birefringent), the attenuation is insignificant and there is a single light source connected to port 1 and K_1 is given by:

$$K_1 = \begin{bmatrix} K_{13} & 0 & K_{14} & 0 \\ 0 & K_{13} & 0 & K_{14} \\ 0 & 0 & 0 & 0 \\ 0 & 0 & 0 & 0 \end{bmatrix}. \tag{9}$$

The transfer function T is expressed by:

$$T = \begin{bmatrix} \exp(i\phi_a) & 0 & 0 & 0 \\ 0 & \exp(i\phi_a) & 0 & 0 \\ 0 & 0 & \exp(i\phi_b) & 0 \\ 0 & 0 & 0 & \exp(i\phi_b) \end{bmatrix}. \tag{10}$$

Since it was assumed that birefringence is absent, the input field may be selected arbitrarily. If $\mathbf{F}_{\text{in}} = (1,0,0,0)$ at the input, the signal received in the detector can be described by [2, 3]:

$$i_1 = 2A_s A_o \cos(\Delta\phi), \tag{11}$$

where i_1 – detector current, A_o – the reference amplitude of the optical wave (arm a), A_s – the signal amplitude of the optical wave (arm b), $\Delta\phi$ – a phase difference expressed as:

$$\Delta\phi = \phi_a - \phi_b, \tag{12}$$

where ϕ_a – the phase shift in the a arm, ϕ_b – the phase shift in the b arm.

3. Principle of operation of the Mach–Zehnder

When ultrasonic vibrations introducing variable stresses into the optical waveguide are delivered to one of the optical fiber arms (the signal arm with length L_s) of the interferometer, a light modulation effect is obtained. The effect is observed on the oscilloscope screen as a signal with frequency modulated by the ultrasonic wave (Fig. 2). The length of the reference arm is L_o. As the result of the vibration, the optical fiber stretches (elongates) and the signal is shifted in phase.

This paper includes measurement results for different methods of delivering ultrasonic waves to the optical fiber, i.e. using radial vibrations of a piezoelectric disk (Fig. 2a) or longitudinal vibrations generated by a sandwich ultrasonic transducer with a velocity transformer (Fig. 2b).

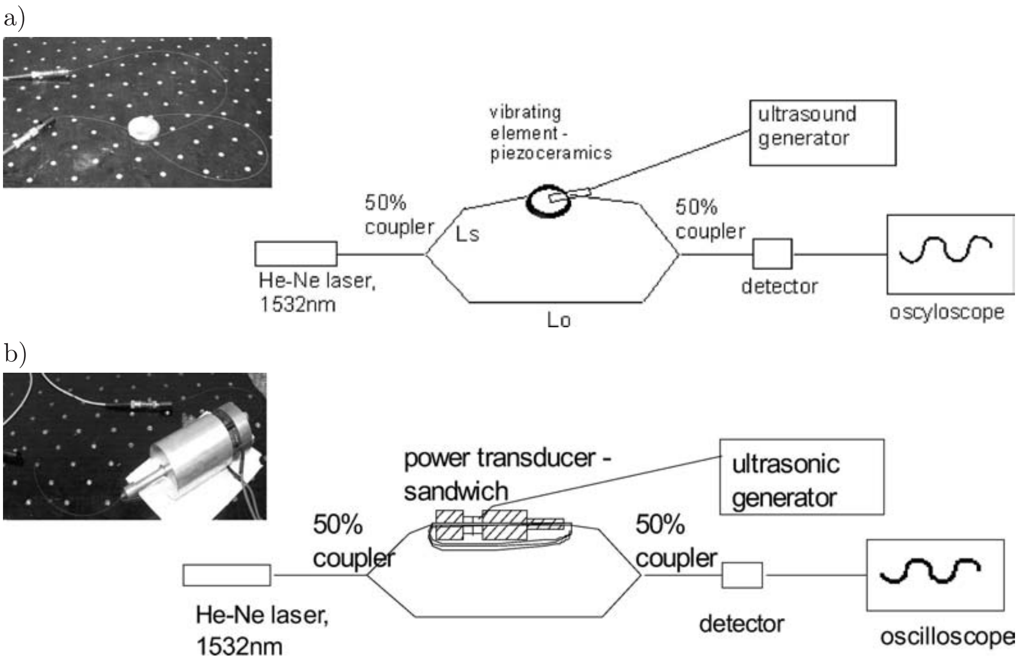

Fig. 2. Mach–Zehnder interferometer with vibrating: a) a piezoelectric disc (radial vibration), b) a power "sandwich" ultrasonic transducer (longitudinal vibration).

4. Measurements by the optical monomode Mach–Zehnder interferometer

When two linearly polarized monochromatic plane waves of the same frequency with amplitudes A_o and A_s interfere, the resulting electric field can be expressed by [3]:

$$E = A_o \exp i\left(\omega t + 2\pi\frac{L_s}{\lambda_0}\right) + A_s \exp i\left(\omega t + 2\pi\frac{L_o}{\lambda_0}\right), \tag{13}$$

where ω – radian frequency of the optical wave, L_s – signal arm length, L_o – reference arm length.

The light intensity can be expressed by:

$$I \approx E_0 E_s^* + E_s E_0^* \approx A_o A_s \cos\left[\Delta\phi\right], \tag{14}$$

where E_0 – electric field in the reference arm, E_s – electric field in the signal arm.

The phase shift $\Delta\phi$ is proportional to the geometrical path difference ΔL and can be expressed by the folowing equation [3]:

$$\Delta\phi = \frac{2\pi}{\lambda_0}(L_s - L_o) = \frac{2\pi}{\lambda_0}L_{(s-o)}. \tag{15}$$

Since the detector current i_1 is proportional to the light intensity:

$$i_1 \sim 2A^2\cos[\Delta\phi] \tag{16}$$

i_1 can be expressed by Eq. (11).

Assuming that the measuring signal influencing the interferometer signal arm can be expressed by [2, 3, 10, 12]:

$$\Delta\phi = \phi_0 + \phi_s \sin\omega_s t, \tag{17}$$

where ϕ_0 – phase shift produced by environmental effects in the fiber, ϕ_s – phase shift in the signal arm caused by the measured signal, one gets information on the useful signal, which can be expressed as $\phi_s \sin\omega_s t$ [9].

The maximum phase excursion ϕ_s caused by fiber stretching can be related to the change in length [4]:

$$\phi_s = \frac{2\pi\xi n\Delta L}{\lambda}, \tag{18}$$

where ΔL – fiber length difference, ξ – a strain optic correction factor (for a silica glass fiber it amounts to 0.78) [4], n – optical refractive index of the medium (1.45), λ – optical wavelength.

The detector current can be expressed by [3, 11]:

$$i_1 = i_o\left\{1 + G\cos[\phi_0 + \phi_s\sin(\omega_s t)]\right\}, \tag{19}$$

where i_o – input current connected with the input optical power, G – visibility of the fringes.

In order to eliminate the influence of the phase ϕ_0 and to get in this way only useful information, the optical interferometer should be located at the point of maximum sensitivity [5–7, 11], i.e. at the point of quadrate expressed by:

$$\phi_0 = \frac{\pi}{2} + m\pi, \tag{20}$$

where m is an integer.

Having transformed the current detector formula by means of trigonometric functions, one gets the following equation [5]:

$$i_1 = i_o \left(1 + G\{\cos\phi_0 \cos[\varphi_s \sin(\omega_s t)] - \sin\phi_0 \sin[\varphi_s \sin(\omega_s t)]\}\right). \tag{21}$$

Taking into account the relation for ϕ_0, one gets the following expression:

$$i_1 = i_o \left(1 - G\{\sin\phi_0 \sin[\phi_s \sin(\omega_s t)]\}\right). \tag{22}$$

Assuming $i_o(1 - G) = 1$, the detector current can be expressed by:

$$i_1 = \sin\left[\phi_s \sin(\omega_s t)\right]. \tag{23}$$

Definition of the stripe:

Stripe $P(t)$ can be called the section of the function:

$$P(t) = i_1(t)\left.\right|_{(t_1,t_2]\subset T}. \tag{24}$$

such that:

1. $i_1(t_1) = i_1(t_2) = 0$ are the only points at which $P(t) = 0$ for each $t \in (t_1, t_2)$,
2. $\forall t \in [t_1, t_2], P(t) > 0$,
3. $\forall P(t)\ \exists t_0 \in [t_1, t_2]$ such that $P(t_0)$ is a local maximum.

If $P(t)$ has only one local maximum, the stripe is unregenerate, otherwise the stripe is referred to as a degenerate stripe.

5. Theoretical graphs plotted in Matlab

Figure 3 shows the dependence of the number of stripes on the frequency for a constant phase shift and on the constant number of fiber turns around the piezoceramic element. The graphs are based on calculations made in Matlab.

From Fig. 3 one can conclude that the number of stripes does not depend on the frequency.

The dependence of the number of stripes and the changes in phase ϕ_s for 1 turn (calculated theoretically in Matlab) is shown in Fig. 5. According to Fig. 4, a change of phase causes a change in the number of stripes [12]. The calculations were performed for a constant number of turns ($n = 1$). One can also notice that the smallest phase difference which can be measured is ϕ_s. The smallest measurable phase difference diminishes with the increase in the number of fiber turns.

a) $f = 64.1$ kHz b) $f = 66.525$ kHz

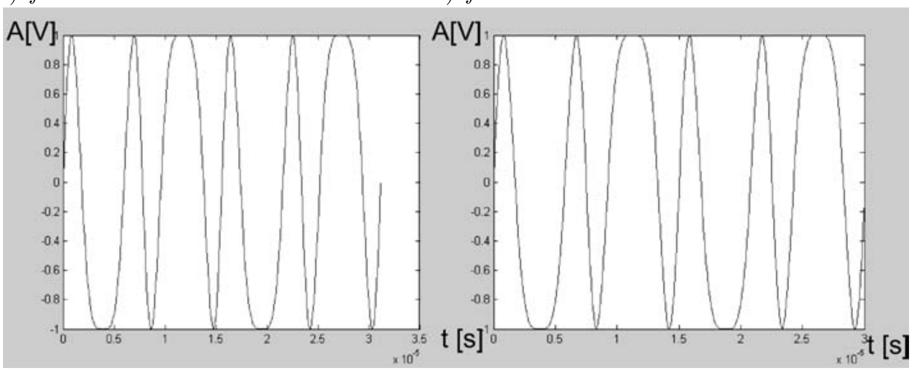

Fig. 3. Dependence between number of stripes and frequency.

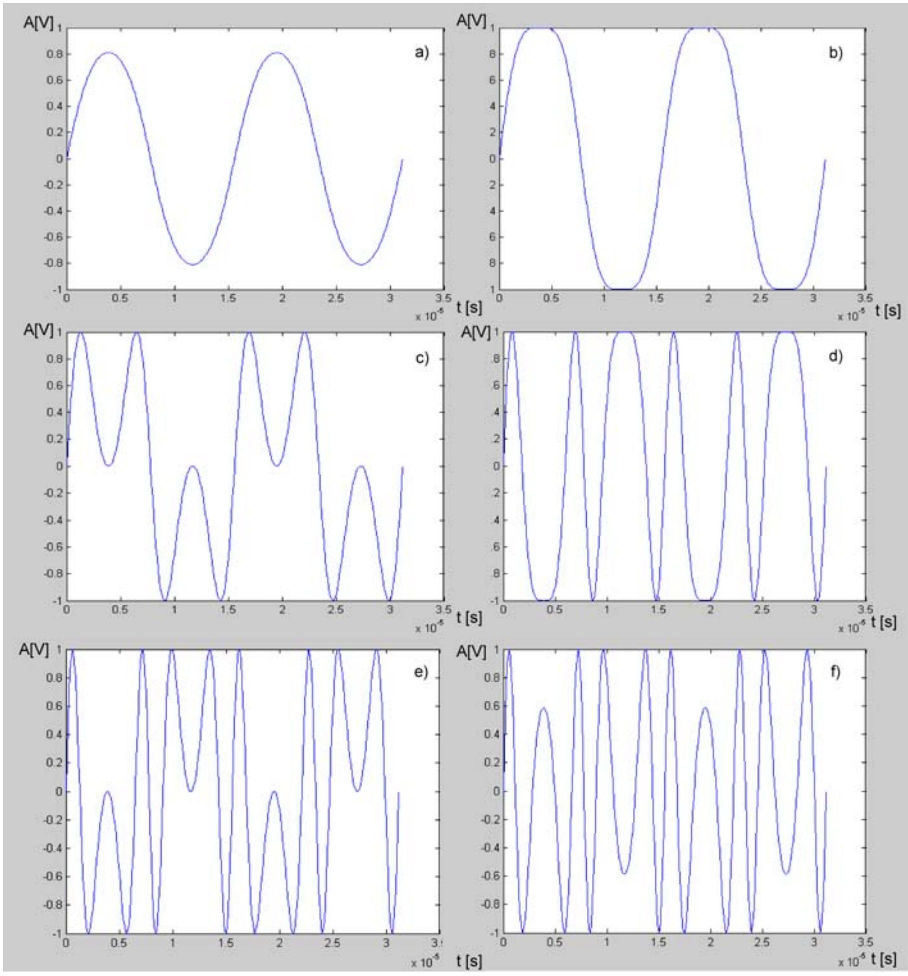

Fig. 4. Dependence of the number of stripes on the changes in phase ϕ_s: a) 0.3 π, b) 0.5 π, c) π, d) 1.5 π, e) 2 π, f) 2.2 π.

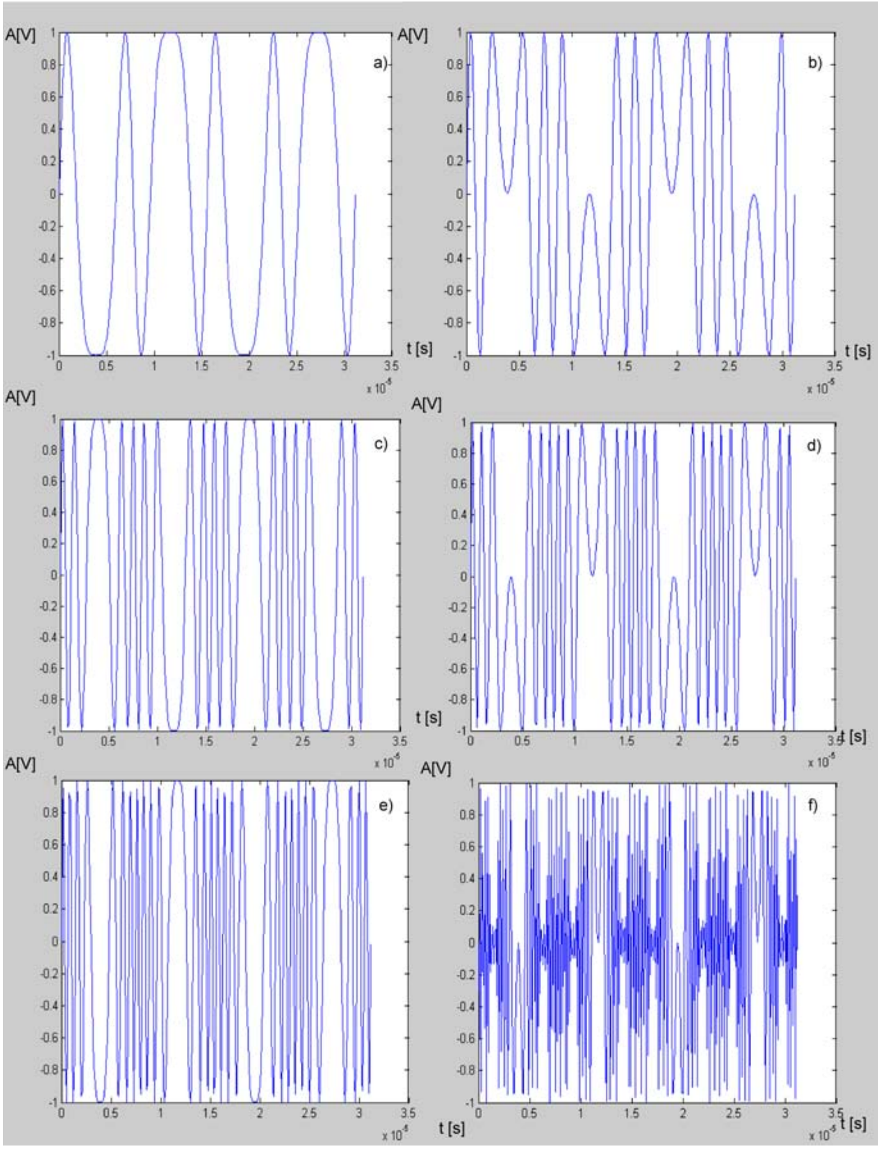

Fig. 5. Dependence of the number of stripes on the number of fiber turns: a) 1 coil, b) 2 coils, c) 3 coils, d) 4 coils, e) 5 coils, f) about 20 coils.

Assuming $\phi_s = 1.5\pi$, one can determine the theoretical number of stripes depending on the number of turns (Fig. 5). The number of stripes increases with the number of fiber turns. For this reason, one should take into account the number of stripes in formula (23):

$$i_1 = \sin(n\phi_s \sin(\omega_s t)), \tag{25}$$

where n – the number of turns.

6. Results of experimental investigations

The frequency at the optical detector output and the frequency of the generator powering the ultrasonic transducer were measured and a linear dependence, confirming the light beam modulation effect produced by the ultrasonic wave propagated in the optical waveguide, was obtained, see Fig. 6.

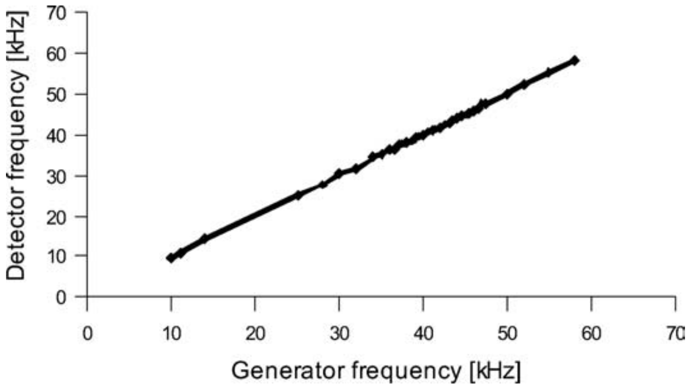

Fig. 6. Frequency at the optical detector output versus frequency of the generator.

The results for the different methods of delivering ultrasonic waves to the optical fiber, i.e. using radial vibrations of a piezoelectric disk or longitudinal vibrations generated by a sandwich ultrasonic transducer with a velocity transformer, are presented below.

6.1. Using radial vibrations of piezoelectric disk

Figure 7 shows the influence of optical fiber cutback precision on the output signal amplitude.

The quality of the connection of optical fibers to the acoustic transducer has a bearing on the occurrence of stripes and on the bandwidth (the very poor impedance match between transducer and air and between air and the optical glass fiber).

One should note that when the optical fiber is firmly fixed to the piezoceramics, the amplitude increases. When there is no good connection, stripes may not appear at all (Fig. 8).

Figure 9 shows the dependence of the bandwidth on the number of fiber turns. One can see that this dependence is approximately linear. The bandwidth in which stripes appear increases with the number of fiber turns.

The results obtained have been compared with the theoretical calculation results. The comparison is presented in Fig. 10.

The graphs based on the calculations and the results for the number of turns equal to 20 are shown on the left and right side, respectively.

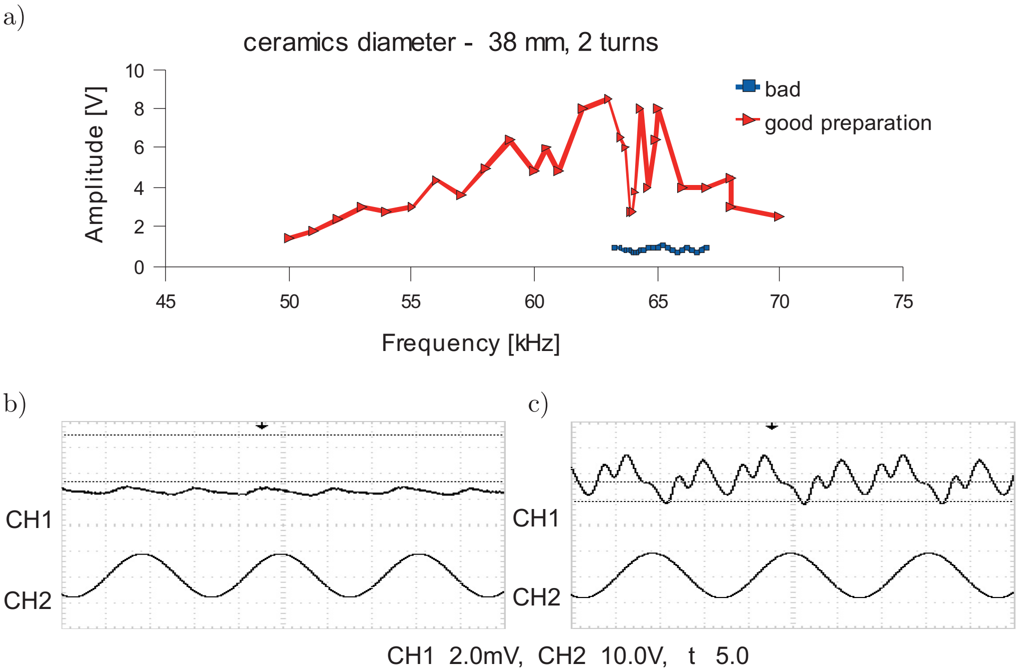

Fig. 7. Influence of the optical fiber cutback precision on the output signal amplitude: a) comparison of amplitudes, b) badly cut off optical fiber, c) well prepared optical fiber.

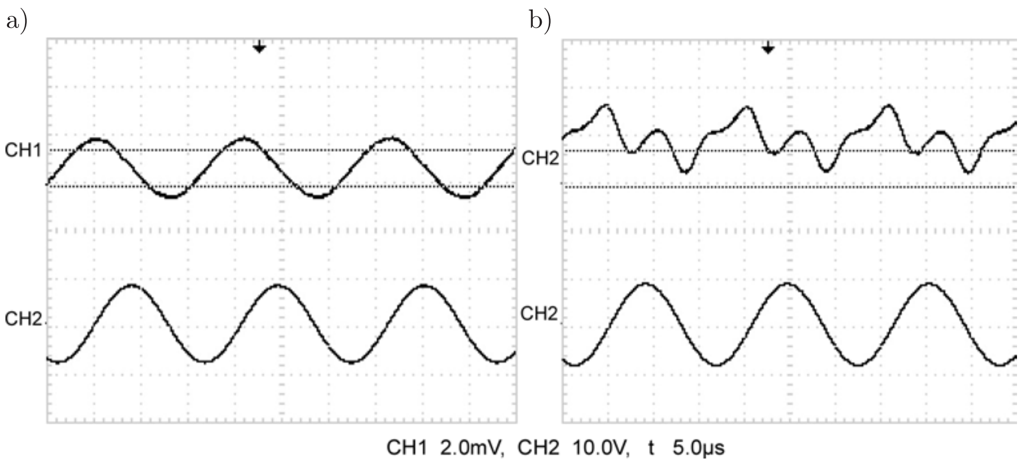

Fig. 8. Dependence of input signal on precision of optical fiber fixing to ceramics (ceramics diameter – 38 mm, 1 turn): a) insufficient fixing, b) proper optical fiber fixing to ceramics.

The number of stripes depends on the number of turns. The larger the number of optical fiber coils on the ceramics, the more stripes appear (Fig. 11). This is confirmed by the theoretical calculations made in Matlab. The Matlab graphs are shown in Fig. 5.

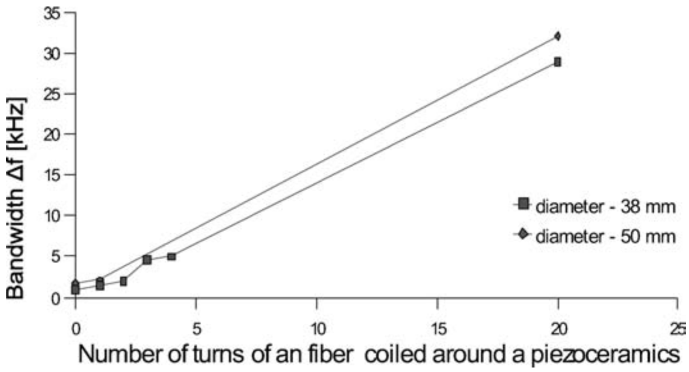

Fig. 9. Dependence of the bandwidth in which stripes appear on the number of fiber turns.

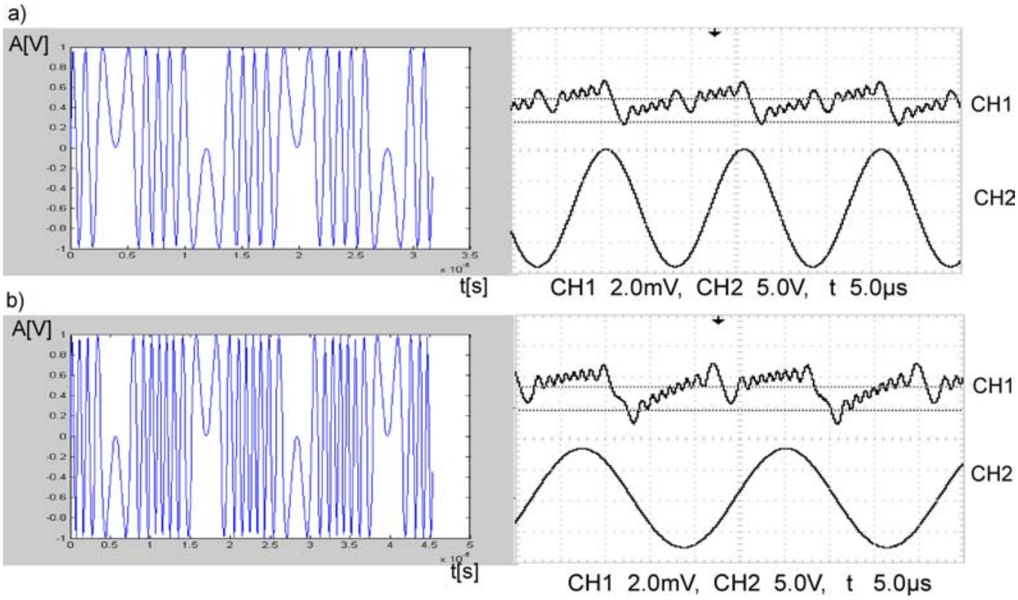

Fig. 10. Comparison of experimental and theoretical calculations: a) phase shift $= 0.25\ \pi$, 10 stripes appeared; b) phase shift $= 0.4\ \pi$, 16 stripes.

Figure 12 represents the dependence of the number of fringes on frequency for various numbers of turns of the fiber around piezoceramics.

For the resonance frequency, the number of fringes is the largest one. Since the number of fringes does not depend on the frequency, this means that the phase shift becomes the largest one for the resonance frequency.

With the growth of the number of turns of the fiber the amplitude falls down and the number of fringes grows (Fig. 13).

Figure 14 shows the dependence of the amplitude on frequency for small and large ceramics. According to the figure, the output signal amplitude is the smallest one for the resonance frequencies. The farther is the frequency from resonance one, the higher the amplitude in which subsequently falls at frequencies distant from the resonance frequencies. The output signal amplitude for the larger ceramics (50 mm diameter) is higher than for the smaller ones (38 mm diameter). The larger the diameter of the ceramics, the higher the vibration of the amplitude.

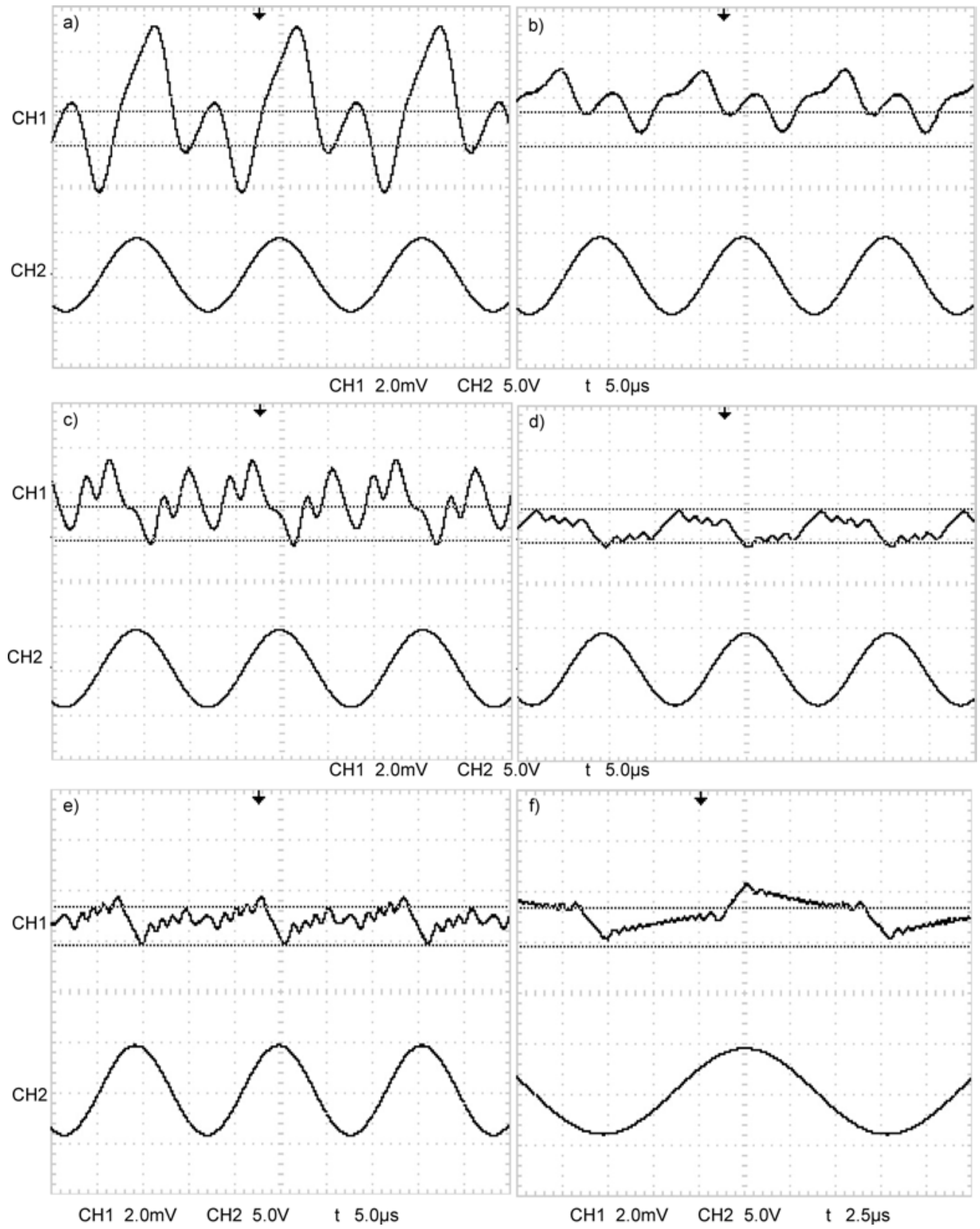

Fig. 11. Dependence of the number of stripes on the number of optical fiber turns: a) 1 coil, b) 2 coils, c) 3 coils, d) 4 coils, e) 5 coils, f) many coils (about 20).

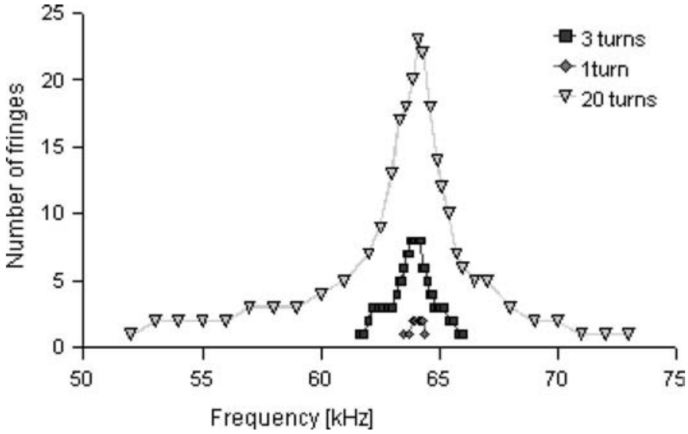

Fig. 12. Dependence of the number of fringes on frequency.

a) b)

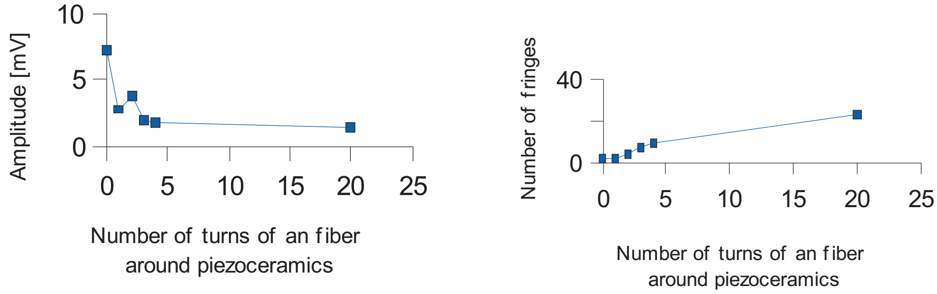

Fig. 13. Dependence of the a) amplitude and b) number of fringes on the number of turns of the fiber.

a) b)

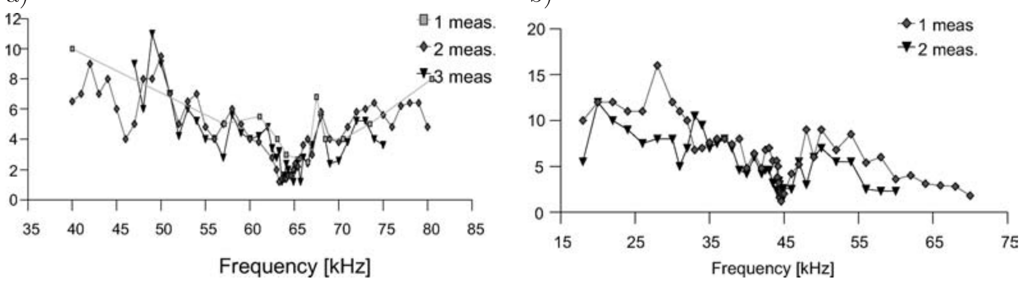

Fig. 14. Output signal amplitude versus the ceramics vibration frequency (many coils): a) diameter 38 mm, b) 50 mm.

In case of smaller ceramics (38 mm diameter), there are two resonances. Figure 15 shows the dependence of the number of stripes on the number of turns for multiple turns at two resonance frequencies: $f_1 = 64.1$ kHz, $f_2 = 66.525$ kHz.

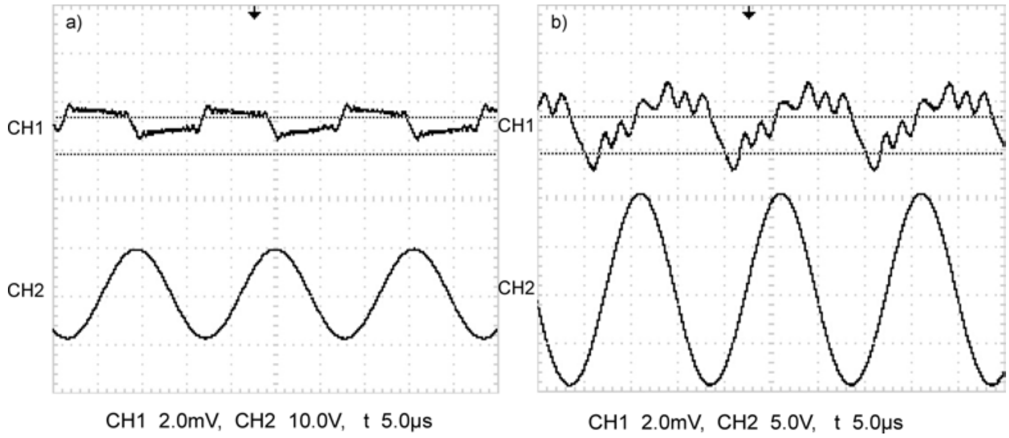

Fig. 15. Comparison of graphs for resonance frequencies: a) $f_1 = 64.1$ kHz, b) $f_2 = 66.525$ kHz.

One can notice that the phase displacement is different for the two resonance frequencies as indicated by the different numbers of stripes.

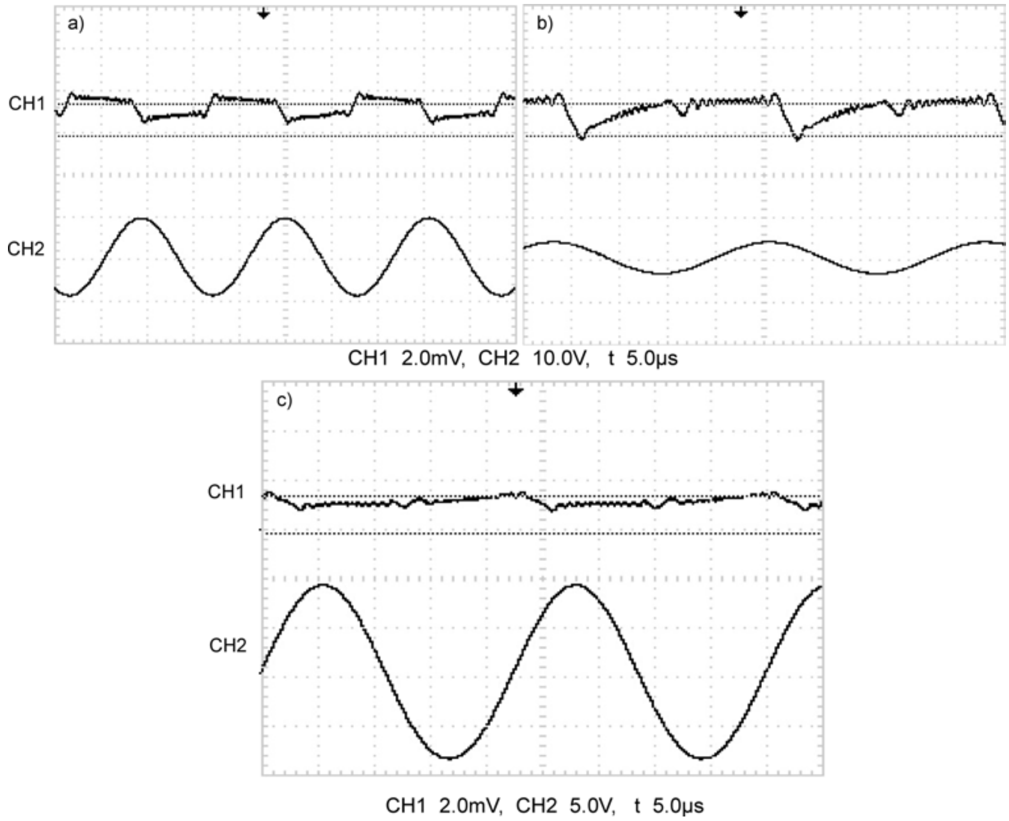

Fig. 16. Dependence of the amplitude on the ceramics dimensions: a) diameter $D = 38$ mm, b) $D = 50$ mm, c) $D = 38$ mm with hole $D = 10$ mm.

A comparison of the number of stripes depending on the dimensions of the ceramics is shown in Fig. 16. The measurements were performed for ceramic diameters of 38 mm and 50 mm and for hollow ceramics (diameter 38 mm). The highest amplitude is observed for the largest ceramics. The output signal amplitude is higher for the non-hollow ceramics than for the hollow ones.

6.2. Using longitudinal vibrations generated by a sandwich ultrasonic transducer with velocity transformer

The signal output amplitude for the optical fiber not firmly connected to the transducer is shown in Fig. 17b. When the optical fiber is stuck to the transducer, the amplitude of the output signal is larger (Fig. 17c). The number of optical turns is equal 1. Figure 17a shows the signal at the detector output when ultrasounds are not applied.

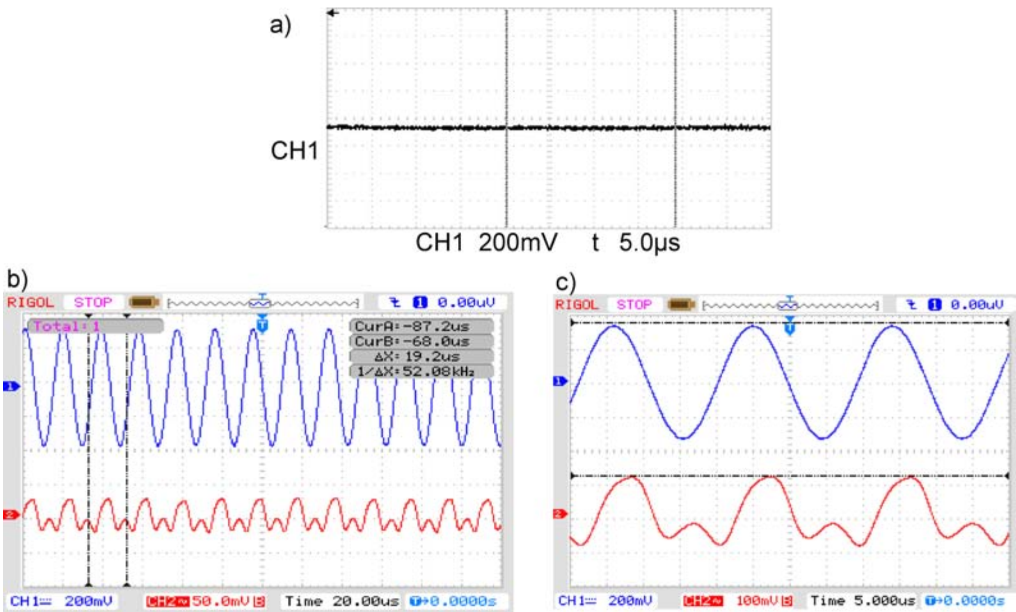

Fig. 17. Output signal amplitude depending on the fiber fixing to the ultrasonic transducer: a) output signal without ultrasonic vibrations, b) optical fiber not firmly connected to transducer, c) firm fixing of the optical fiber to the transducer.

A full match between the signal frequency received by the detector and the resonance frequency of the ultrasonic transducers was obtained. The output signal amplitude increases with power. The amplitude for the frequency of 52.5 kHz is higher than that for the frequency of 50.6 kHz. The ultrasonic transducer works better on the frequency of 52.5 kHz (Fig. 18). Measurements were performed for a constant number of turns ($n = 1$), and for the power $P = 1$ W.

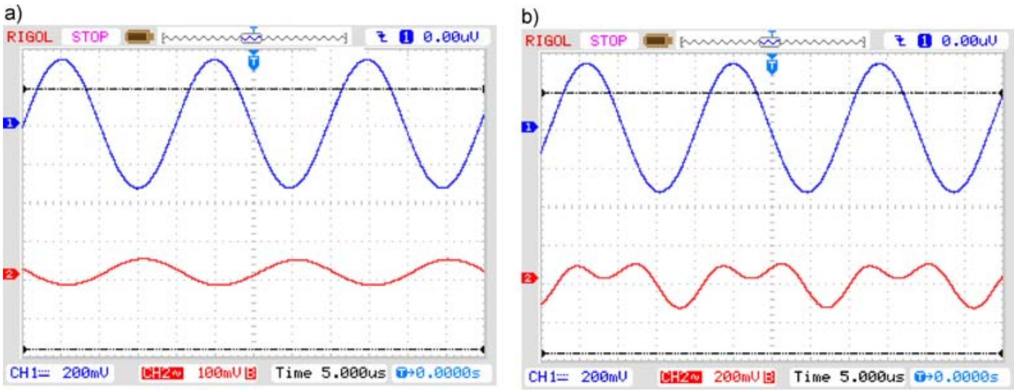

Fig. 18. Comparison of graphs for resonance frequencies: a) $f = 50.6$ kHz, b) $f = 52.5$ kHz.

The experiment carried out showed, that the number of stripes depends on the number of turns also for the power sandwich ultrasonic transducer (Fig. 19). Power delivered to the transducer was $P = 4$ W for the frequency $f = 52.5$ kHz.

The investigations were conducted for powers delivered to the transducer ranging from 5 to 54 W.

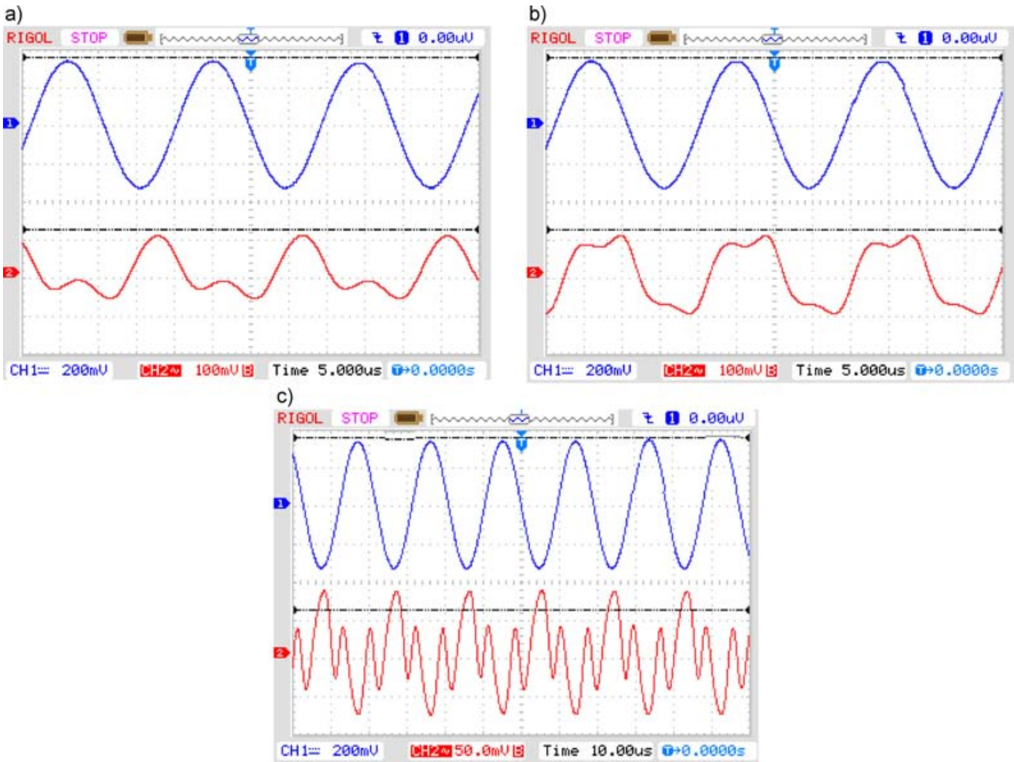

Fig. 19. Dependence of the number of stripes on the number of optical fiber turns: a) 1 coil, b) 2 coils, c) 3 coils.

7. Conclusion

In order to get an effective combination of the laser and ultrasonic technologies, the light and the ultrasounds must properly interact. It has been shown that at a low frequency, high power ultrasonic transmission in fibers by means of a sandwich ultrasonic transducer is possible. In a single-mode waveguide, acoustic wave propagates in the core and in the cladding [13, 15].

The methods of modulation of a light wave propagating in an optical fiber by means of an ultrasonic wave, which is performed with the use of radial vibrations of a piezoelectric disk and longitudinal vibrations generated by a sandwich ultrasonic transducer with a wave velocity transformer, have been presented. The obtained experimental results presented in this workare agreeable with theoretical considerations. In connection with the conducted preliminary theoretical analysis of the possibilities of compensating for the faults of laser technology and ultrasonic technology in surgery, the combination of laser and ultrasounds in one device seems more effective. The presented research results will serve as the basis for further research of the possibilities [1, 14, 15] of simultaneous high-power laser and ultrasound transmission via flexible glass fibers.

References

[1] Gudra T., Muc S., *A preliminary analysis of possibilities of compensating faults of laser and ultrasonic technologies is surgery*, Archives of Acoustics, **32**, 4 (Supplement), 117–122 (2007).

[2] Jackson D.A., Jones J.D.C., *Fibre optic sensors*, Optica Acta, **33**, 12, 1469–1503 (1986).

[3] Grattan K.T.V., Megitt B.T., *Optical Fibre Sensor Technology*, Chapman & Hall, London 1995.

[4] Spammer S.J., Swart P.L., *Differentiating optical-fibre Mach–Zehnder interferometer*, Appl. Opt., **34**, 13, 2350–2353 (1995).

[5] Udd E. [Ed.], *Fiber Optic Sensors: An Introduction for Engineers and Scientists*, Willey, New York 2006.

[6] Dandridge A., *et al.*, *Overview of Mach–Zehnder Sensor Technology and Applications*, SPIE, Fiber Optic and Laser Sensors VI, **1985**, 34–52 (1998).

[7] Jackson D.A., *Monomode optical fibre interferometers for precision measurement*, J. Phps. E: Sci. Instrum., **18**, 981–1001 (1985).

[8] Giallorenzi T.G., Bucaro J.A., Dandridge A., Sigel G.H. Jr., Cole J.H., Rashleigh S.C., Priest R.G., *Optical Fiber Sensor Technology*, IEEE Journal of Quantum Electronics, **QE-18**, 4, April 1982.

[9] Kingsley S.A., Davies D.E.N., *Multimode optical-fibre phase modulators and discriminators: I-theory*, Electronics Letters, **14**, 11, 322–324, 25th May 1978.

[10] Carome E.F., Koo K.P., *PVF2 phase shifters and modulators for fiber optic sensor systems*, Ultrasonics Symposium, 710–712 (1980).

[11] Tribikram Kundu, *Ultrasonic Nondestructive Evaluation: Engineering and Biological Material Characterization*, 7 chapter (Sridhar Krishnaswamy, Theory and Applications of Laser-Ultrasonic Techniques, pp. 436–489), CRC Press, 2004.

[12] Kotov O.I., Liokumovich L.B., Markov S.I., Medvedev A.V., Khlybov A.V., *Modulation of the Phase Difference between Polarization Modes in Single-Mode Fiber Light Guides*, Technical Physics, **49**, 1, 71–75 (2004).

[13] Muc S., *Experimental study of transmission of ultrasonicwave in optical fibers*, Archives of Acoustics, **33**, 4, 619–625 (2008).

[14] Gudra T., Muc S., *Some problems of ultrasonic and laser cutting of biological structures*, Eur. Phys. J. Special Topics, **154**, 85–88 (2008).

[15] Muc S., Gudra T., Bereś–Pawlik E., *Methods of modulation of light wave propagated in optical fiber using ultrasonic wave*, ICU '2009 (paper presented on ICU '2009).